Urol Res (2012) 40:121–129
DOI 10.1007/s00240-011-0400-z

ORIGINAL PAPER

Role of osteopontin in early phase of renal crystal formation: immunohistochemical and microstructural comparisons with osteopontin knock-out mice

Masahito Hirose · Keiichi Tozawa · Atsushi Okada · Shuzo Hamamoto · Yuji Higashibata · Bin Gao · Yutaro Hayashi · Hideo Shimizu · Yasue Kubota · Takahiro Yasui · Kenjiro Kohri

Received: 15 August 2009 / Accepted: 30 June 2011 / Published online: 11 August 2011

Abstract Osteopontin (OPN) is an important matrix protein of renal calcium stone. However, the function of OPN in the early phase of renal crystal formation is not well defined. In this study, we examined OPN expression in the early phase of renal crystal formation with ultra-microstructural observations and immuno-TEM (transmission electron microscopy) in control and OPN knock-out (OPN-KO) mice. Glyoxylate (100 mg/kg) was intra-abdominally administered to male wild-type mice (C57BL/6, 8 weeks of age) and OPN-KO mice (C57BL/6, 8 weeks of age). Kidney was collected before and 6, 12, and 24 h after administration. We examined the relation between renal crystal formation and microstructural OPN location using TEM and immunohistochemical staining of OPN as well as western blotting and quantitative RT-PCR for OPN. OPN protein expression gradually increased in the renal cortex-medulla junction after glyoxylate administration, and OPN mRNA was increased until 12 h, but decreased at 24 h. In ultra-microstructural observation, OPN began to appear on the luminal side of renal distal tubular cells at 6 h and was gradually detected in the tubular lumen at 12 h. OPN was present in the crystal nuclei and collapsed mitochondria in the tubular lumen. In the OPN-KO mice, collapsed mitochondria were present, but no crystal nuclei formation were detected at 24 h. Based on the results this study proposed that the appearance of organelles, such as mitochondria and microvilli, in the tubular lumen after cell injury may be the starting point of crystal nucleus formation due to the aggregation ability of OPN.

Keywords Renal stone · Osteopontin · Osteopontin knock-out mice · Glyoxylate · Electron microscopy

M. Hirose · K. Tozawa (✉) · A. Okada · S. Hamamoto · Y. Higashibata · Y. Hayashi · Y. Kubota · T. Yasui · K. Kohri
Department of Nephro-Urology, Nagoya City University Graduate School of Medical Sciences, 1 Kawasumi, Mizuho-cho, Mizuho-ku, Nagoya 467-8601, Japan
e-mail: toza@med.nagoya-cu.ac.jp

B. Gao
School of Basic Medical Science, Shenyang Medical College, 110034 Shenyang, China

B. Gao
China-Japan Kidney Stone Research Center, 146 Huanghe North Street, 110034 Shenyang, China

H. Shimizu
Core Laboratory Division, Nagoya City University Graduate School of Medical Sciences, 1 Kawasumi, Mizuho-cho, Mizuho-ku, Nagoya, Japan

Introduction

Renal stone disease is a common clinical disorder, and calcium oxalate (CaOx) is the principal crystalline component in approximately 75% of all renal stones. CaOx stones contain various urinary components, and albumin, globulin, Tamm-Horsfall glycoprotein (THP), prothrombin fragment 1, inter-α-trypsin inhibitor (bikunin), osteopontin (OPN), and calprotectin have also been reported [1–3]. These components are termed crystal matrix proteins and constitute 1–5% of urinary stones. Several studies have suggested the importance of proteins in stone formation [4, 5].

We have previously cloned and sequenced the cDNA encoding OPN, an important soluble protein component of CaOx stone proteins, after extracting it with 0.1 M ethylenediamine tetraacetic acid (EDTA) [6]. The multifunctional protein OPN is secreted by various cell types and is involved in diverse biological processes, including inflammation, leukocyte recruitment, wound healing, and cell

injury [7–11]. OPN is present in many tissues, including bone, kidneys, gall bladder, pancreas, lungs, breast, and salivary, and sweat glands [12, 13]. It is also produced in culture by certain kidney cell lines, including MDCK, LLCPK-1, and cortical cells [14]. Subsequently, we found strong OPN mRNA expression in distal renal tubular cells (RTC) in the kidneys of stone-forming rats [15].

OPN is also involved in biological calcification, with osteoclast-derived OPN acting to inhibit hydroxyapatite formation during normal bone mineralization [16]. In addition, macrophage and smooth muscle cell-derived OPN is associated with dystrophic calcification in degenerative and atheromatous vascular disease, with in vitro data suggesting an inhibitory action on such calcification [17–20]. OPN is synthesized within the kidney and is present in human urine at levels that can effectively inhibit CaOx crystallization [21–23]. Indeed, reduced concentrations of OPN have been documented in urine from patients with renal stone disease compared with normal individuals [24, 25]. In vitro data indicate that urinary OPN may inhibit the nucleation, growth, and aggregation of CaOx crystals in cultured renal epithelial cells [26–28].

Another indication of OPN involvement in stone formation comes from its ubiquitous presence in stones, where it is a major component of the organic matrix and appears to be associated with crystals early in formation [29, 30]. In our previous study [31, 32], the CaOx crystals formed by intra-abdominal injection of glyoxylate for 3–6 days in OPN knock-out (OPN-KO) mice were found to be smaller than those in wild-type mice.

Despite these numerous in vitro studies, there is little currently available data to indicate whether OPN or any of the other individual urinary macromolecules are necessary to prevent or promote stone formation in vivo.

In this study, we investigated the role of OPN in the early phase of renal crystal formation in renal crystal formation model mice and OPN-KO mice by immunohistochemical staining and ultra-microstructure observation using transmission electron microscopy (TEM). This study of microstructural OPN location and movement in the early stage of crystal formation is the first report to examine OPN in the context of early stage of renal stone formation.

Methods

Animals

The experimental animals were male wild-type mice (C57BL/6, 8 weeks of age) and OPN-KO mice (C57BL/6, 8 weeks of age) weighing 18–22 g [31]. The mice were housed in metabolic cages for 7 days before the experiment for acclimation. The ambient temperature was maintained at 23 ± 1°C on a 12-h light/dark cycle. All animals had free access to standard chow (including calcium 1.12 g, phosphorus 0.9 g, magnesium 0.26 g, and sodium 0.21 g/100 g; Oriental Yeast, Tokyo, Japan) and water.

All animal studies followed the recommendations of the NIH Guidelines for the Care and Use of Laboratory Animals.

All experiments proceeded with the approval of the Animal Care Committee of the Faculty of Medicine, Nagoya City University Graduate School of Medical Sciences.

Experimental protocols

Twenty-eight wild-type mice and 28 OPN-KO mice were administered glyoxylate (Wako, Tokyo, Japan) with intra-abdominal injection (100 mg/kg (1.35 mmol/kg)). The glyoxylate was stored at 4°C until administration. Kidney tissues were extracted before and 6, 12, and 24 h after glyoxylate administration ($n = 7$ at each time point).

OPN examination

Western blotting ($n = 7$ at each time point)

For whole-protein extraction from the kidney specimens, we used the cell culture lysis reagent (Promega Corp., Madison, WI, USA) according to the manufacturer's instructions. In brief, frozen kidney tissue was immersed in 1× lysis buffer and sonicated on ice for a sufficient duration. Following incubation on ice for 15 min, the suspension was centrifuged, the supernatant collected, and the total protein concentration quantified on a spectrophotometer using the bicinchoninic acid protein assay reagent (Pierce Biotechnology, Rockford, IL, USA). Samples containing 30 μg total protein were mixed with loading buffer (Laemmli sample buffer, Bio-Rad Laboratories, Hercules, CA, USA). They were then boiled for 10 min at 100°C, run on a 10% sodium dodecyl sulfate–polyacrylamide gel electrophoresis (SDS-PAGE) gel for protein resolution, and transferred onto polyvinylidene difluoride (PDVF) membranes (Immobilon, Millipore Corp., Bedford, MA, USA). The membranes were then blocked with 5% skim milk in Tris-buffered saline (pH 7.5) containing Tween 20 (TBS-T) for 1 h at room temperature and sequentially incubated with polyclonal anti-mouse OPN rabbit IgG (IBL Co., Ltd., Gunma, Japan) at 4°C overnight. After the membranes were washed with TBS-T, they were incubated with the corresponding peroxidase-conjugated Peroxidase Labeled Anti-Rabbit IgG (H + L) Antibody (Kirkegaard & Perry Laboratories, Inc. Washington, DC, USA) at room temperature for 1 h and subsequently washed once again with TBS-T. The protein bands were visualized using enhanced chemiluminescence (ECL)

western blotting analysis kits (Pierce Biotechnology), according to the manufacturer's instructions.

Quantitative RT-PCR (n = 7 at each time point)

Total RNA was isolated from frozen sections of mouse kidney samples with ISOGEN (Nippon Gene Co., Ltd., Toyama, Japan), according to the manufacturer's instructions. Applied Biosystems' TaqMan Gene Expression Assay (Applied Biosystems, Foster City, CA, USA), 20× assay mix of primers, and TaqMan MG probes (FAM dye-labeled), for OPN mRNA (Mm00436767_m1, Applied Biosystems) were used for quantitative RT-PCR [31] using the ABI PRISM7700 Sequence Detection System (Applied Biosystems). This assay was designed to span exon–exon junctions so as not to detect genomic DNA, and these primers and probe sequences were searched for against the Celera database to confirm their specificity. Validation experiments were performed to test the efficiencies of the target and reference amplifications. OPN mRNA amplification was compared with the amplification of standard oligo-DNA fragments that had been prepared previously by RT-PCR using the same primer sets, and their concentrations were determined. Absolute copy numbers were determined with a standard curve and corrected with the amount of total RNA. One-Step RT-PCR reactions using the TaqMan One-Step RT-PCR Master Mix Reagent Kit (4309169, Applied Biosystems) were started with an initial reverse transcription step at 48°C for 30 min. After denaturing at 95°C for 10 min, the PCR was started at 95°C for 15 s and completed at 60°C for 1 min. The PCR reaction was repeated 40 times. The reaction components consisted of 25 µl of 2× Master Mix, 1.25 µM of 40× MultiScribe and RNase Inhibitor Mix, 2.5 µl of OPN expression quantitative primer, and 400 ng/ml total RNA sample. The internal control was a GAPDH primer.

Immunohistochemical staining using light microscopy and confocal microscopy (n = 7 at each time point)

Immunohistochemical staining, viewed by light microscopy, was carried out in sections treated with microwaves for 15 min and blocked with 0.5% H_2O_2 in methanol for 30 min before being washed in 0.01 M phosphate-buffered saline (PBS) and further treated with skimmed milk in PBS for 1 h at room temperature. These slides were then incubated with polyclonal anti-mouse OPN rabbit IgG (IBL Co., Ltd., Gunma, Japan). The reacted antibody was detected using a VECTASTAIN Elite ABC kit for rabbit IgG (Vector Laboratories, Inc. Burlingame, CA, USA) according to the manufacturer's instructions.

To detect OPN, sections were treated in the same manner until the step involving the primary antibody but having omitted the 0.5% H_2O_2 blocking step. The slides were washed with PBS, then incubated with Alexa Fluor® 488 goat anti-rabbit IgG (H + L) (Life Technologies Japan Ltd., Tokyo, Japan) at room temperature for 1 h followed by 4′,6-diamidino-2-phenylindole dihydrochloride (DAPI) (Life Technologies Japan Ltd.) at room temperature for 30 min to stain the nucleus. OPN fluorescence was detected using a Leica DMI4000 B (Leica Microsystems, Tokyo, Japan).

Immunohistochemical staining using TEM (n = 7 at each time point)

Immunohistochemical staining of the microstructure was examined by TEM. Perfusion fixation was performed with 20 ml 0.1 M phosphoric acid buffer and 20 ml 4% paraformaldehyde, and kidney tissue was extracted. The kidney tissue was soaked in 4% paraformaldehyde overnight, before being washed in sucrose solutions with a concentration gradient from 10 to 20%. Dehydration was performed in a series of ethanol concentrations (50–100%). The kidney tissue was embedded gradually in a series of LR-White (London Resion Co., Ltd, Hampshire, UK) solutions from 50 to 100% (diluted ethanol). Polymerization was performed at 4°C for 48 h in the TUV-200 (Dosaka EM Co., Ltd, Kyoto, Japan). After making super slice pieces (99 nm), the pieces were placed on carbon-coated 200 mesh nickel grids (JEOL Ltd., Tokyo, Japan). Each grid was etched with 10% H_2O_2 for 30 min before being washed three times in 0.01 M phosphate-buffered saline (PBS) and further treated with skimmed milk in PBS for 30 min at room temperature. Subsequently, the grids were incubated overnight with polyclonal anti-mouse OPN rabbit IgG (IBL Co., Ltd., Gunma, Japan) at 4°C. Each grid was rinsed three times in PBS. The secondary antibody was goat anti-rabbit IgG-Gold Colloidal Particles-15 nm (EY Laboratories, Inc., San Mateo, CA, USA). Each grid was rinsed three times in PBS. For contrast, the grids were stained with uranyl acetate and lead citrate before being observed by JEM -1011 (JEOL Ltd., Tokyo, Japan).

Microstructural observation of kidney (n = 7 at each time point)

Microstructure observation was performed using TEM. Perfusion fixation was performed with 20 ml of 0.1 M phosphoric acid buffer and 20 ml of 2.5% glutaraldehyde, and the kidney tissue was extracted. The kidney tissue was washed with a phosphoric acid buffer, and fixation was then performed with 2% osmium liquid for 2 h. Dehydration was performed using a series of ethanol concentrations (50–100%). Renal tissue was embedded in epoxy resin. Polymerization was performed at 60°C for 48 h. After making each super slice piece (99 nm), double staining was

performed with uranium and lead, and then the super slice was observed using a JEM -1011 (JEOL Ltd., Tokyo, Japan).

Statistical analysis

The OPN mRNA expression values obtained by quantitative RT-PCR are expressed as means ± SD. Statistical analysis was performed using the Mann–Whitney *U* test. A probability of 0.05 was considered significant.

Results

Western blotting for OPN

OPN protein expression in wild-type mice is shown in Fig. 1a. Before glyoxylate treatment, OPN expression was shown slightly. After treatment, OPN expression increased gradually in a time-dependant manner. In OPN-KO mice kidney, OPN expression was not detected at all time points (date not shown).

Quantitative RT-PCR for OPN

OPN mRNA expression is shown in Fig. 1b. OPN expression increased significantly at 6 h after glyoxylate administration (about 8 times greater than before glyoxylate treatment, $P = 0.017$). At 12 h, OPN expression was increased 24 times as compared with before glyoxylate treatment ($P = 0.02$), and 3 times as compared with the 6-h group ($P = 0.017$). At 24 h, OPN expression was increased two times compared with before glyoxylate treatment ($P = 0.019$), and decreased one-twelfth compared with the 12-h group. In OPN-KO mice kidney, OPN expression was not detected at all time points.

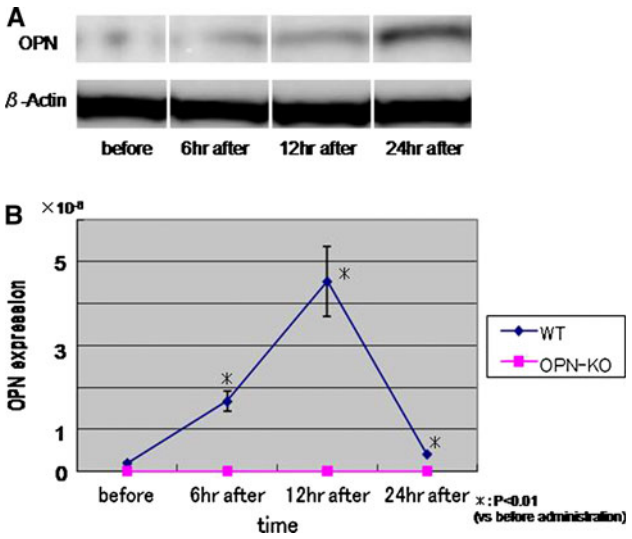

Fig. 1 Western blotting and Quantitative RT-PCR of OPN. **a** Western blotting, **b** quantitative RT-PCR. Data are expressed as mean ± SD

Immunohistochemistry of OPN using light microscopy and confocal microscopy in Fig. 2

OPN expression was slightly detected in distal RTC of before glyoxylate treatment mice kidneys. In the kidneys of glyoxylate-treated mice after 6 h, OPN expression was increased in the distal RTC of the renal medulla and cortex-medulla junction as compared with the control mice. OPN was detected, in particular, in the luminal side of RTC, and not detected in the cytoplasm, nucleus, and interstitial space. The increase in OPN expression was greater at 12 h as compared with 6 h, and was detected in and around the luminal side of RTC. At 24 h, OPN expression was greater than at 12 h, and was detected in the lumen of dilated RTC, but not in the cytoplasm, nucleus, or interstitial space. In OPN-KO mice kidney, OPN expression was not detected at all time points (date not shown).

Immunohistochemistry of OPN using TEM

OPN was not detected in the distal RTC prior to glyoxylate treatment (Fig. 3a *x*, *y*). OPN expression increased around luminal side of the distal RTC in glyoxylate-treated kidney after 6 h (Fig. 3b *x*, *y*). In particular, OPN was detected near the collapsed RTC and mitochondria, which had acquired an indistinct internal structure and double membrane. After 12 h, OPN expression was detected together with cell debris in the lumen of distal RTC (Fig. 3c *x*, *y*). After 24 h, OPN expression was detected in the lumen of the expanding distal RTC (Fig. 3d *x*, *y*). In the lumen, OPN was detected together with collapsed mitochondria and crystal nuclei (Fig. 3e *x*, *y*-1, *z*). OPN was detected particularly around crystal nuclei in the lumen (Fig. 3e *y*-2).

Observation of cell microstructure in OPN-KO mice

Prior to glyoxylate treatment, the RTC microvilli (Fig. 4a *x*) were tall, and present in high density. The mitochondria (Fig. 4a *y*) were arranged orderly, with clearly defined, continuous double membranes. The internal structure of the mitochondria was arranged regularly.

After 6 h, the microvilli had been reduced to few in number and had shortened (Fig. 4b *x*). The mitochondrial internal structure, and the clarity and continuity of the mitochondrial membrane, had become slightly indistinct (Fig. 4b *y*).

After 12 h, most of the microvilli had become shorter, and the lumen had expanded slightly (Fig. 4c *x*). Some of

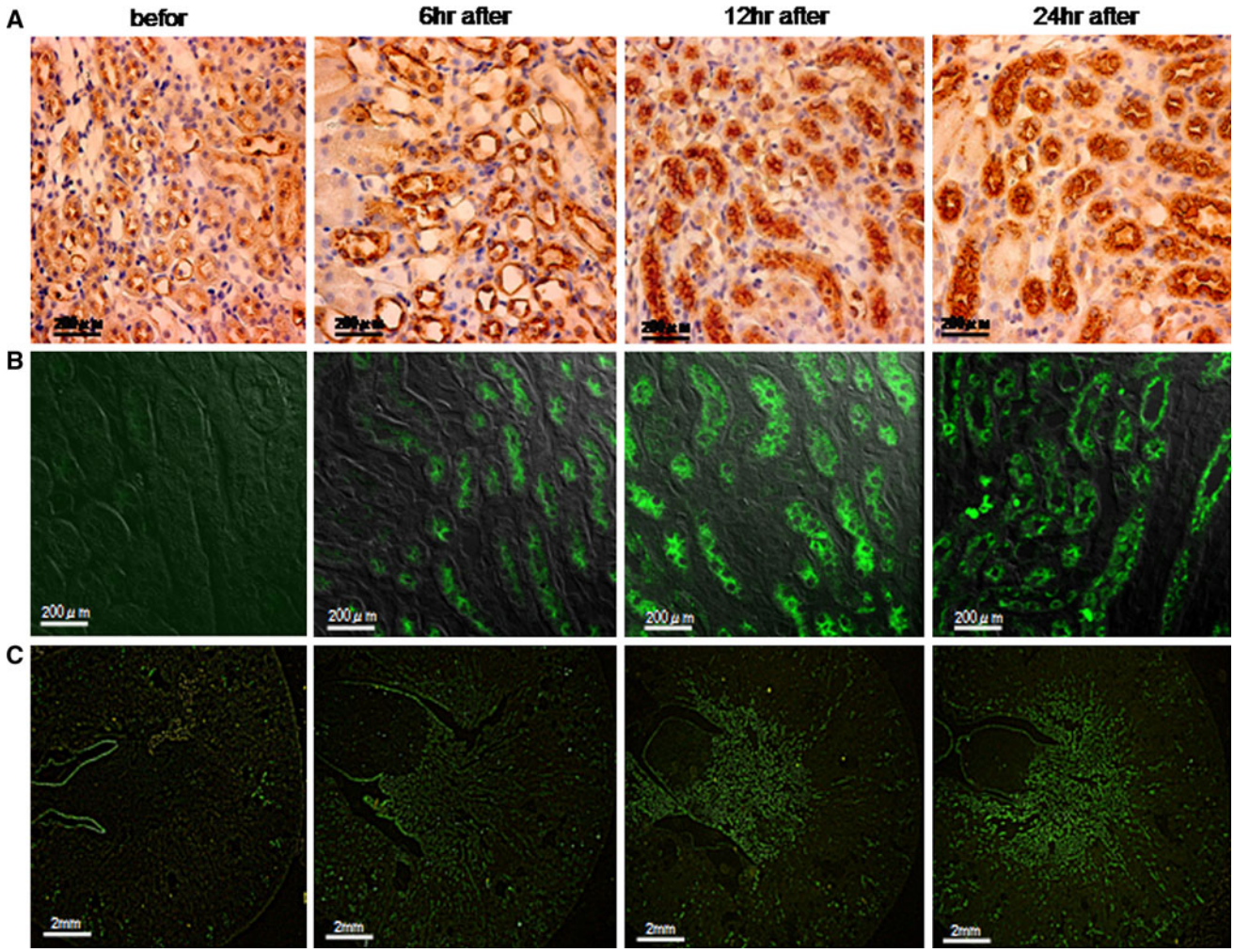

Fig. 2 Immunohistochemistry of OPN using light microscopy and confocal microscopy. **a** Light microscopy magnification ×400, **b** confocal microscopy magnification ×400, **c** confocal microscopy magnification ×40

the microvilli disappeared and appeared in the lumen. The membrane of the mitochondria (Fig. 4c *y*) had lost its continuity and clarity. The internal structure of the mitochondria was indistinct. The mitochondria in the lumen showed little internal structure or double membrane.

After 24 h, only a few mitochondria were observed in each cell, and most of the microvilli had disappeared (Fig. 4d *x*, *y*). There were many mitochondria in the lumen. The mitochondria had collapsed and showed traces of the double membrane and the internal structures (Fig. 4d *y*). Some mitochondria showed fat droplet transformation, and vacuolization, but no crystal nuclei were detected (Fig. 4d *x*).

Discussion

In the present study, we examined that OPN expression increased prior to crystal formation in the renal medulla and cortex-medulla junction. OPN began to appear on the luminal side of the distal RTC and gradually appeared in the tubular lumen, accompanied by collapsed microvilli and mitochondria. OPN was present in the nuclei of CaOx crystals in the tubular lumen.

OPN has been reported to promote stone formation, based on elevated OPN mRNA levels in stone-forming rats [33, 34] and its promotion of CaOx crystal adherence to MDCK cells [26–28]. However, OPN has also been reported to be an inhibitor of stone formation, based on its inhibitory effect on the formation/aggregation/growth of CaOx crystals in an in vitro study [35, 36]. In our previous study using OPN-KO mice, we reported [31] that OPN was essential for the growth, fixation, and structural arrangement of CaOx stones in the mouse kidney. And OPN-KO mice formed a few crystals less than WT mice after 3 days in renal cortex-medulla junction. OPN is reportedly related to human kidney stones [37, 38]. Evan et al. reported [39] that OPN is one of the crystal-associated urine proteins

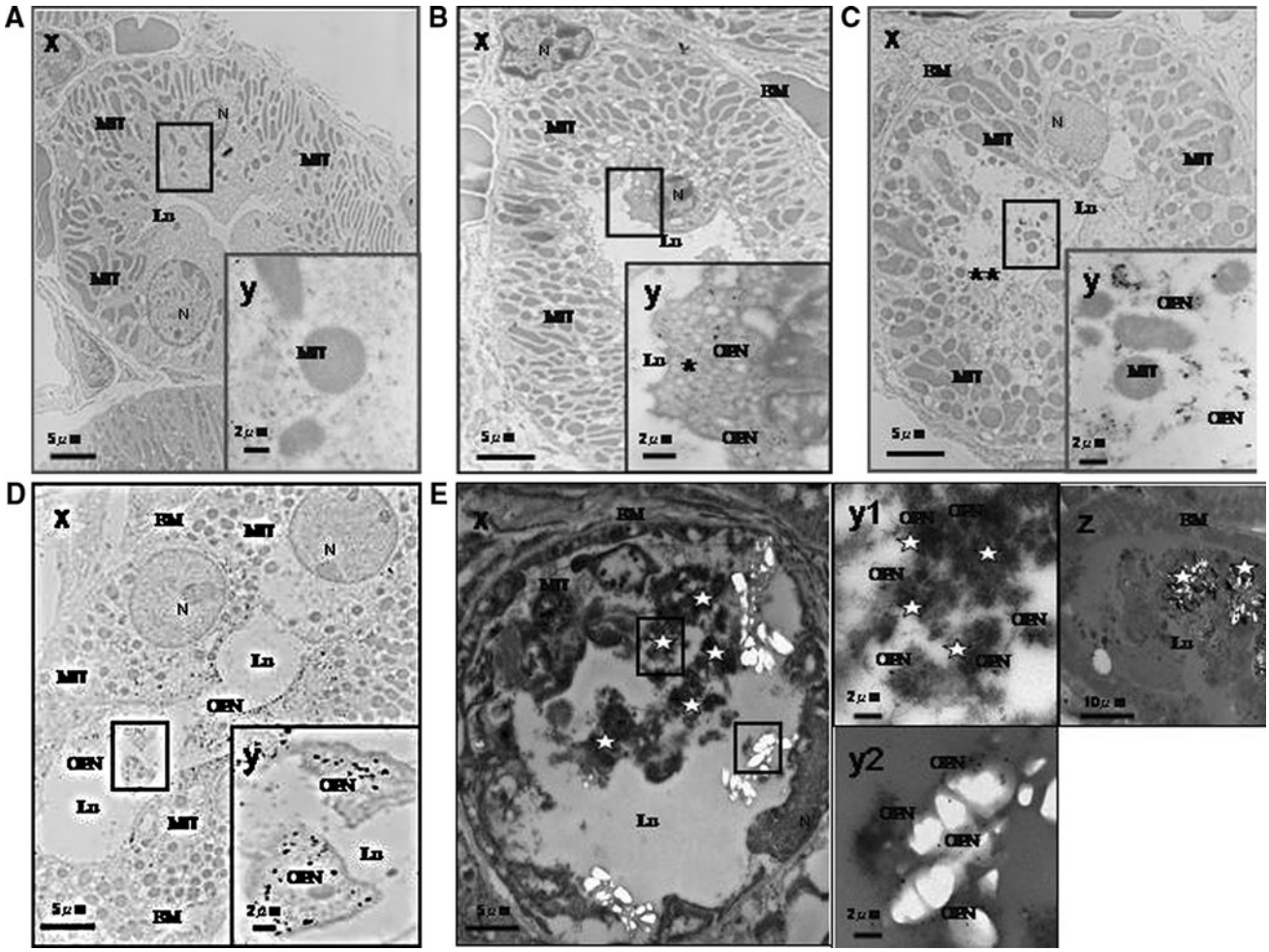

Fig. 3 Immunohistochemistry of OPN using TEM. Crystal nuclei had been present (**e** *x*, *y*-1, *z*) (*z*: 0.5 μm slices), but then the parts have fallen out after becoming dislodged from the 99-nm slices (**e** *x*, *y*-2). The RTC microstructural form in the immunohistochemical study using TEM was more indistinct than in normal TEM study as glutaraldehyde was not used for fixation, because although glutaraldehyde has a strong fixation effect, it is at the expense of antigenicity. *Asterisk* collapsed RTC. *Double asterisk* cell debris. *Star* crystal nuclei. *N* nucleus, *MV* microvilli, *BM* basement membrane, *Lu* renal tubular lumen, *MIT* mitochondria (magnification *x*, *z*: ×5,000, *y*: ×20,000)

involved in the formation of the organic layers of human kidney plaque particles. However, the detailed morphological relationship between the early period of crystal formation and OPN function is unclear.

In this study, we clarified the OPN-associated morphological changes in RTC during the early period of CaOx crystal formation in glyoxylate administrated mice. In our previous study [40, 41], RTC injury and oxidative stress were detected 6 h after glyoxylate administration, indicating that cell injury and oxidative stress occur prior to crystal formation. We proposed that the crystal formation mechanism occurs as follows: Glyoxylate administration induces RTC transformation during the early period of CaOx crystal formation. Consequently, the mitochondria and microvilli of the RTC relocated gradually into the lumen as a result of RTC injury. The mitochondria in the lumen of the distal RTC caused calcification and aggregation. The organelles, such as mitochondria and microvilli, in the renal tubular lumen form the nuclei of the crystals.

We proposed the following regarding the relationship between OPN and cell injury in the early period of crystal formation. Cell injury is caused by glyoxylate administration, which then causes OPN expression in the lumen of distal RTC prior to CaOx crystal formation. In the lumen, OPN may aggregate cell debris and form crystal nuclei. This study supports a previous study [31, 32], which showed that OPN is essential for the growth, fixation, and structural arrangement of CaOx crystals in the mouse kidney, and we proposed that OPN is necessary for the early period of crystal formation. Interestingly, OPN is reported to be involved in both inflammation and

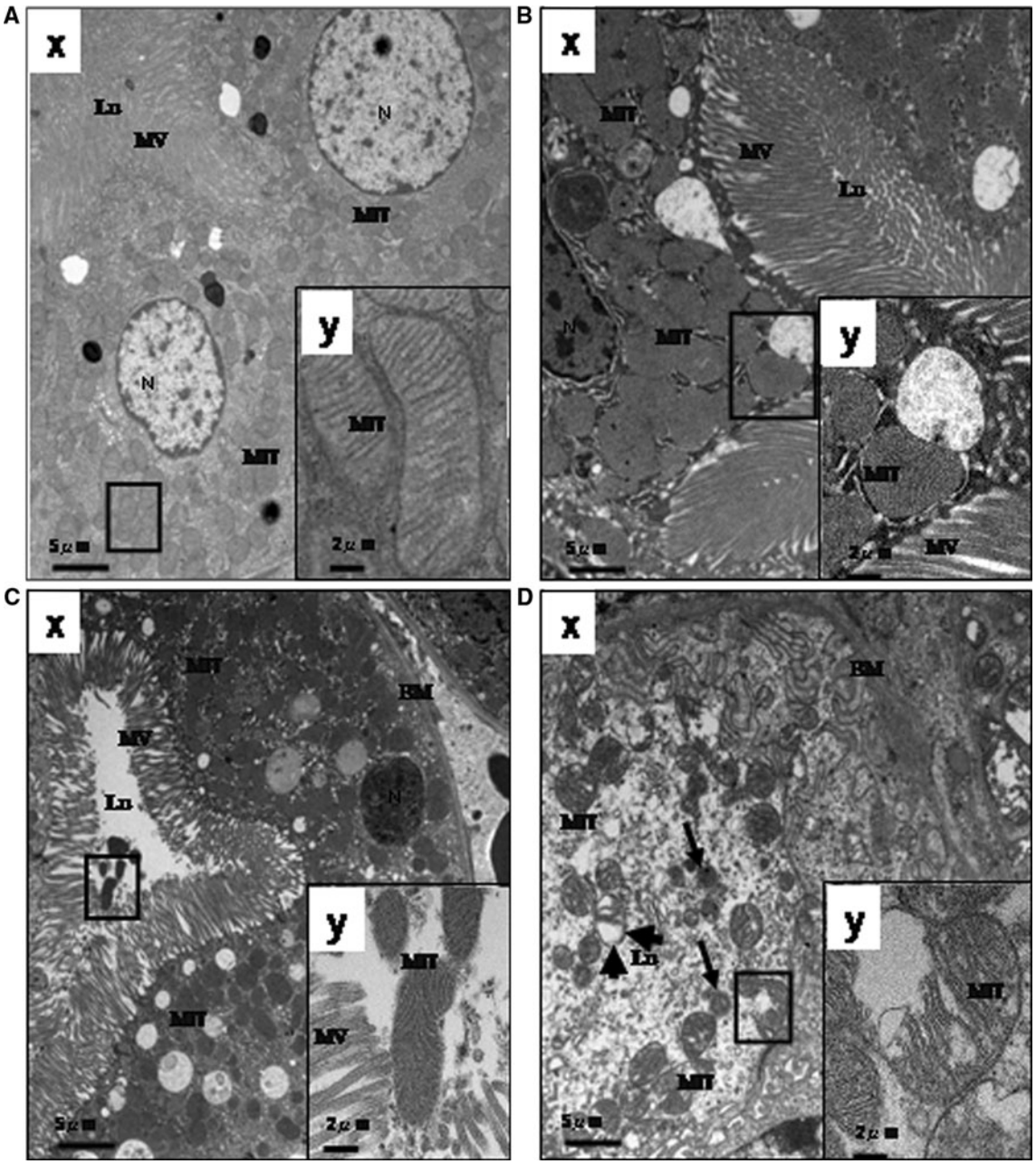

Fig. 4 Observation of the cell microstructure in OPN-KO mice. *Arrows*: fat droplet transformation of mitochondria. *Arrow heads*: vacuolization of mitochondria. *N* nucleus, *MV* microvilli, *BM* basement membrane, *Lu* renal tubular lumen, *MIT* mitochondria (magnification a: ×5,000, b: ×20,000)

leukocytoplania at the sites of tissue injury [42], as well as playing a role in calcium binding and cell interactions [32, 43].

In conclusion, the appearance of organelles, such as mitochondria and microvilli, in the tubular lumen after cell injury may be the starting point of crystal nucleus formation due to the aggregation ability of OPN, leading to the development of renal stones. This study evaluated the OPN expression during the early period of crystal formation and supported the proposed pathogenesis of CaOx crystal formation induced by RTC injury. This study emphasizes the importance of OPN in the pathogenesis of renal stones.

Acknowledgments We would like to thank Ms. N. Kasuga, Ms. A. Hayashi, and Ms. Y. Kobayashi for their expert management of the mice and secretarial assistance. This work was supported, in part, by Grants-in-Aid from the Ministry of Education, Culture, Science, and Technology (No. 18209050, No. 18791132, No. 21791519).

References

1. Kulaksizoglu S, Sofikerim M, Cevik C (2007) Impact of various modifiers on calcium oxalate crystallization. Int J Urol 14:214–218
2. Mo L, Liaw L, Evan AP et al (2007) Renal calcinosis and stone formation in mice lacking osteopontin, Tamm-Horsfall protein, or both. Am J Physiol Renal Physiol 293:1935–1943
3. Khan SR (2004) Crystal-induced inflammation of the kidneys: results from human studies, animal models, and tissue-culture studies. Clin Exp Nephrol 8:75–88
4. Canales BK, Anderson L, Higgins L et al (2008) Second prize: comprehensive proteomic analysis of human calcium oxalate monohydrate kidney stone matrix. J Endourol 22:1161–1167
5. Merchant ML, Cummins TD, Wilkey DW et al (2008) Proteomic analysis of renal calculi indicates an important role for inflammatory processes in calcium stone formation. Am J Physiol Renal Physiol 295:F1254–F1258
6. Kohri K, Suzuki Y, Yoshida K et al (1992) Molecular cloning and sequencing of cDNA encoding urinary stone protein, which is identical to osteopontin. Biochem Biophys Res Commun 184:859–864
7. O'Brien ER, Garvin MR, Stewart DK et al (1994) Osteopontin is synthesized by macrophage, smooth muscle, and endothelial cells in primary and restenotic human coronary atherosclerotic plaques. Arterioscler Thromb 14:1648–1656
8. Giachelli CM, Lombardi D, Johnson RJ et al (1998) Evidence for a role of osteopontin in macrophage infiltration in response to pathological stimuli in vivo. Am J Pathol 152:353–358
9. Liaw L, Birk DE, Ballas CB et al (1998) Altered wound healing in mice lacking a functional osteopontin gene (spp1). J Clin Invest 101:1468–1478
10. Ophascharoensuk V, Giachelli CM, Gordon K et al (1999) Obstructive uropathy in the mouse: role of osteopontin in interstitial fibrosis and apoptosis. Kidney Int 56:571–580
11. Scatena M, Almeida M, Chaisson ML et al (1998) NF-kappaB mediates alphavbeta3 integrin-induced endothelial cell survival. J Cell Biol 141:1083–1093
12. Brown LF, Berse B, Van de Water L et al (1992) Expression and distribution of osteopontin in human tissues: widespread association with luminal epithelial surfaces. Mol Biol Cell 3:1169–1180
13. Kleinman JG, Beshensky A, Worcester EM et al (1995) Expression of osteopontin, a urinary inhibitor of stone mineral crystal growth, in rat kidney. Kidney Int 47:1585–1596
14. Itoh Y, Yasui T, Okada A et al (2005) Examination of the antioxidative effect in renal tubular cells and apoptosis by oxidative stress. Urol Res 33:261–266
15. Kohri K, Nomura S, Kitamura Y et al (1993) Structure and expression of the mRNA encoding urinary stone protein (osteopontin). J Biol Chem 268:15180–15184
16. Pampena DA, Robertson KA, Litvinova O et al (2004) Inhibition of hydroxyapatite formation by osteopontin phosphopeptides. Biochem J 378:1083–1087
17. O'Brien KD, Kuusisto J, Reichenbach DD et al (1995) Osteopontin is expressed in human aortic valvular lesions. Circulation 92:2163–2168
18. Srivatsa SS, Harrity PJ, Maercklein PB et al (1997) Increased cellular expression of matrix proteins that regulate mineralization is associated with calcification of native human and porcine xenograft bioprosthetic heart valves. J Clin Invest 99: 996–1009
19. Ikeda T, Shirasawa T, Esaki Y et al (1993) Osteopontin mRNA is expressed by smooth muscle-derived foam cells in human atherosclerotic lesions of the aorta. J Clin Invest 92: 2814–2820
20. Wada T, McKee MD, Steitz S et al (1999) Calcification of vascular smooth muscle cell cultures: inhibition by osteopontin. Circ Res 84:166–178
21. Kleinman JG, Beshensky A, Worcester EM et al (1995) Expression of osteopontin, a urinary inhibitor of stone mineral crystal growth, in rat kidney. Kidney Int 47:1585–1596
22. Asplin JR, Arsenault D, Parks JH et al (1998) Contribution of human uropontin to inhibition of calcium oxalate crystallization. Kidney Int 53:194–199
23. Min W, Shiraga H, Chalko C et al (1998) Quantitative studies of human urinary excretion of uropontin. Kidney Int 53:189–193
24. Nishio S, Hatanaka M, Takeda H et al (2000) Calcium phosphate crystal-associated proteins: alpha2-HS-glycoprotein, prothrombin F1, and osteopontin. Mol Urol 4:383–390
25. Nishio S, Hatanaka M, Takeda H et al (1999) Analysis of urinary concentrations of calcium phosphate crystal-associated proteins: alpha2-HS-glycoprotein, prothrombin F1, and osteopontin. J Am Soc Nephrol 10:394–396
26. Yamate T, Kohri K, Umekawa T et al (1996) The effect of osteopontin on the adhesion of calcium oxalate crystals to Madin-Darby canine kidney cells. Eur Urol 30:388–393
27. Lieske JC, Leonard R, Toback FG (1995) Adhesion of calcium oxalate monohydrate crystals to renal epithelial cells is inhibited by specific anions. Am J Physiol 268:F604–F612
28. Yamate T, Kohri K, Umekawa T et al (1998) Osteopontin antisense oligonucleotide inhibits adhesion of calcium oxalate crystals in Madin-Darby canine kidney cell. J Urol 160:1506–1512
29. McKee MD, Nanci A, Khan SR (1995) Ultrastructural immunodetection of osteopontin and osteocalcin as major matrix components of renal calculi. J Bone Miner Res 10:1913–1929
30. Ryall RL, Grover PK, Thurgood LA et al (2007) The importance of a clean face: the effect of different washing procedures on the association of Tamm-Horsfall glycoprotein and other urinary proteins with calcium oxalate crystals. Urol Res 35:1–14
31. Okada A, Nomura S, Saeki Y et al (2008) Morphological conversion of calcium oxalate crystals into stones is regulated by osteopontin in mouse kidney. J Bone Miner Res 23:1629–1637
32. Hamamoto S, Nomura S, Yasui T et al (2009) Effects of impaired functional domains of osteopontin on renal crystal formation: analyses of OPN-transgenic and OPN-knockout mice. J Bone Miner Res 25:2712–2723
33. Umekawa T, Yamate T, Amasaki N et al (1995) Osteopontin mRNA in the kidney on an experimental rat model of renal stone formation without renal failure. Urol Int 55:6–10
34. Umekawa T, Kohri K, Kurita T et al (1995) Expression of osteopontin messenger RNA in the rat kidney on experimental model of renal stone. Biochem Mol Biol Int 35:223–230
35. Hoyer JR, Otvos L Jr, Urge L (1995) Osteopontin in urinary stone formation. Ann N Y Acad Sci 760:257–265
36. Umekawa T (1999) Structural characteristics of osteopontin for calcium oxalate crystal. Jpn J Urol 90:436–444
37. Ryall RL, Chauvet MC, Grover PK (2005) Intracrystalline proteins and urolithiasis: a comparison of the protein content and ultrastructure of urinary calcium oxalate monohydrate and dihydrate crystals. BJU Int 96:654–663
38. Kleinman JG, Wesson JA, Hughes J (2004) Osteopontin and calcium stone formation. Nephron Physiol 98:43–47
39. Evan AP, Coe FL, Rittling SR et al (2005) Apatite plaque particles in inner medulla of kidneys of calcium oxalate stone formers: osteopontin localization. Kidney Int 68:145–154
40. Hirose M, Yasui T, Okada A et al (2009) Renal tubular epithelial cell injury and oxidative stress induce calcium oxalate crystal formation in mouse kidney. Int J Urol 17:83–92

41. Hirose M, Tozawa K, Okada A et al (2008) Glyoxylate induces renal tubular cell injury and microstructural changes in experimental mouse. Urol Res 36:139–147
42. Vernon HJ, Osborne C, Tzortzaki EG et al (2005) Aprt/Opn double knockout mice: osteopontin is a modifier of kidney stone disease severity. Kidney Int 68:938–947
43. Nakamura I, Duong le T, Rodan SB et al (2007) Involvement of alpha(v)beta3 integrins in osteoclast function. J Bone Miner Metab 25:337–344